Revised Version

DESY 08-079
SFB/CPP-08-33
CERN-PH-TH/2008-138
HU-EP-08/21

On cutoff effects in lattice QCD from short to long distances

ALPHA Collaboration

Michele Della Morte[a], Rainer Sommer[b] and Shinji Takeda[c]

[a] CERN, Physics Department, TH Division, CH-1211 Geneva 23, Switzerland

[b] DESY, Platanenallee 6, 15738 Zeuthen, Germany

[c] Institut für Physik, Humboldt Universität, Newtonstr. 15, 12489 Berlin, Germany

Abstract

We discuss kinematical enhancements of cutoff effects at short and intermediate distances. Starting from a pedagogical example with periodic boundary conditions, we switch to the case of the Schrödinger functional , where the theoretical analysis is checked by precise numerical data with $N_{\rm f} = 2$ dynamical O(a)-improved Wilson quarks. Finally we present an improved determination of the renormalization of the axial current in that theory.

Key words: Lattice QCD; Symanzik effective theory; Non-perturbative renormalization

PACS: 11.10.Gh; 11.15.Ha; 11.40.Ha; 12.38.Gc

July 2008

arXiv:0807.1120v2 [hep-lat] 22 Jul 2008

1 Introduction

Dynamical fermion simulations with Wilson-type fermions are now possible at small quark masses, large volumes [1–8] and small lattice spacings. With statistical precision reaching the (sub-)percent level, an important uncertainty which remains to be carefully controlled is due to the finite lattice spacing a. In the non-perturbatively O(a)-improved theory, this issue has been investigated in some detail. On the one hand, significant a-effects have been found at lattice spacings of around $a = 0.1\,\mathrm{fm}$ [9, 10]. On the other hand, both in the high precision computations of the scale dependence of coupling, quark masses and other composite operators [11–13] (see ref. [14] for a review) and in a recent scaling test [15], such effects were not visible.

In this paper we analyse this apparent contradiction and find that the difference is of a simple kinematical origin, teaching us a more general lesson. In order to keep a-effects small, it is important to ensure that the general conditions necessary for the application of the Symanzik expansion of lattice observables in powers of a are well fulfilled. We discuss the general issue in Sect. 2 and then illustrate it in Sect. 3 on a particular example where precise non-perturbative results are available: a Schrödinger functional correlation function. The lessons we learn there allow us to perform an improved computation of the renormalization of the axial current in Sect. 4, which we check further by considering modified renormalization conditions (Sect. 4.2) before we conclude.

2 The Symanzik expansion and kinematics

Symanzik's effective theory [16–18] is the fundamental tool for analysing the approach of renormalized lattice observables, O_{lat} to their continuum limit O_{cont}. As an example consider the asymptotic expansion of a (space-momentum zero) correlation function (e.g. eq. (2.2))

$$C_{\mathrm{lat}}(x_0, a) \quad \overset{a\to 0}{\sim} \quad C_{\mathrm{cont}}(x_0) + a\, C_1(x_0) + a^2\, C_2(x_0) \; + \ldots \; .$$

The functions C depend in addition to the kinematical argument x_0 on the intrinsic scale $\Lambda \equiv \Lambda_{\mathrm{QCD}} = \mathrm{O}(300\,\mathrm{MeV})$ of the theory as well as the quark masses M_i. In the above formula the powers of the lattice spacing, are in principle modified by a further a-dependence in $C_i(x_0) \to C_i(x_0, a)$. It is a consequence of the dependence of the couplings in the Symanzik effective Lagrangian on a as well as the dependence of the coefficients of the effective fields on a. However, since QCD is asymptotically free, these coefficients depend only logarithmically on the lattice spacing when it is small. Such logarithmic terms are of minor importance for our discussion; they are dropped here.

2.1 Point-to-point correlators at short distances

Let us assume a large volume and a "point-to-point" correlator, i.e. $C_{\mathrm{lat}}(x_0, a) = a^3 \sum_{\mathbf{x}} \langle \mathcal{O}_1(0) \mathcal{O}_2(x) \rangle$ with local operators $\mathcal{O}_{1,2}$. We focus on the short distance regime,

$x_0 \ll 1/\Lambda\,, x_0 \ll 1/M_i$ and an O(a)-improved theory where $C_1 \equiv 0$. Then x_0 provides the only dimensionful parameter. On purely dimensional ground the leading correction then becomes

$$a^2\, C_2(x_0) \quad \stackrel{a\to 0}{\sim} \quad \text{const.} \times (a/x_0)^2\, C_{\rm cont}(x_0)\,. \tag{2.1}$$

It is enhanced at small x_0. In other words what we have used here is that up to logarithmic corrections the short distance correlation functions have a unique power-law behaviour in x_0.

A particularly simple example is

$$C^{\rm PP}_{\rm lat}(x_0,a) = -a^3 \sum_{\mathbf{x}} \langle P^a(0)\, P^a(x)\rangle\,, \quad \text{with} \quad P^a(x) = \overline{\psi}(x)\gamma_5 \tfrac{1}{2}\tau^a \psi(x)\,, \tag{2.2}$$

which one may, in principle, consider for renormalizing the pseudo–scalar density. One expects that the short distance behaviour $C^{\rm PP}_{\rm cont} \sim \text{const.} \times x_0^{-3}$ is difficult to reproduce accurately on a lattice. In fact, *one* term in the Symanzik expansion originates from an O(a^2) correction to the field

$$P^a_{\rm eff}(x) = P^a(x) + a^2 c_2\, \partial^*_\mu \partial_\mu P^a(x) + \ldots \tag{2.3}$$

which contributes

$$C^{\rm PP}_2(x_0)\, a^2 \quad \stackrel{a\to 0}{\sim} \quad 24\, c_2 \frac{a^2}{x_0^2}\, C^{\rm PP}_{\rm cont}(x_0) + \ldots \tag{2.4}$$

to eq. (2.1). An order of magnitude enhancement is due to the second derivative of the steep function $C_{\rm cont}$. Even if c_2 may be arising only at 1-loop of perturbation theory[1], the considered case suffices to illustrate our main point: cutoff effects may have a significant kinematical enhancement. Particular examples are correlation functions with strong short distance singularities.

Of course, this is the reason why the connection between the perturbative short distance regime of QCD and the non-perturbative long distance one is carried out recursively in the strategy of our collaboration [14,19,20]. It is then possible to have $a/x_0 \ll 1$ *and* $x_0\Lambda \ll 1$. But furthermore, by making use of Schrödinger functional boundary conditions [21], one may easily construct correlators with a weak time-dependence [22]. Let us discuss this relevant issue in some more detail.

2.2 Schrödinger functional correlators

We now assume a finite volume with Dirichlet boundary conditions at $x_0 = 0$ and $x_0 = T$ as explained in refs. [18,21,23]. These allow for the definition of gauge invariant boundary fields, for instance

$$\mathcal{O}^a = \frac{a^6}{L^3} \sum_{\mathbf{x}} \sum_{\mathbf{y}} \overline{\zeta}(\mathbf{x})\, \gamma_5\, \tfrac{1}{2}\tau^a\, \zeta(\mathbf{y}) \tag{2.5}$$

[1] this means $c_2 \sim \text{const.}\,/\log(a\Lambda)$

constructed from the boundary quark (and anti-quark) fields ζ ($\overline{\zeta}$) at $x_0 = 0$. In space we use periodic boundary conditions with a phase θ,

$$\psi(x + \hat{k}L) = \mathrm{e}^{i\theta}\,\psi(x)\,, \quad \overline{\psi}(x + \hat{k}L) = \mathrm{e}^{-i\theta}\,\overline{\psi}(x)\,. \tag{2.6}$$

Because of the zero momentum projection of the boundary fields, the correlator

$$f_{\mathrm{lat}}^{\mathrm{P}}(x_0, a) = -\frac{L^3}{6}\langle \mathcal{O}^a\, P^a(x)\rangle \tag{2.7}$$

has a smooth behaviour at short distances (and small L) of the form

$$f_{\mathrm{cont}}^{\mathrm{P}}(x_0) = 3\mathrm{e}^{-2\sqrt{3}\theta\, x_0/L}\,\left\{1 + \mathrm{O}(\bar{g}^2(L)\right\}\,, \tag{2.8}$$

in QCD with 3 colors and for massless quarks. There is no kinematical enhancement of a-effects. Together with the smooth background field introduced for the definition of the running coupling [23, 24], this explains the very small lattice spacing effects in the running coupling and running operators mentioned before.

We may also discuss the behaviour at large distances. There a saturation by few intermediate states in the spectral decomposition (see ref. [25] for a discussion of w, E)

$$f_{\mathrm{lat}}^{\mathrm{P}}(x_0) = \text{const.} \sum_{n,m} w_{nm} \mathrm{e}^{-x_0 E_n^{\pi} - (T - x_0)\, E_m^{\mathrm{vac}}} \tag{2.9}$$

will give an accurate description of the correlation function. The energies E_n^{π} are the finite volume eigenvalues of the QCD Hamiltonian in the pion sector and E_m^{vac} are the energies of states with vacuum quantum numbers. Their dependence on L and the lattice spacing is suppressed. If the kinematics, given by θ, x_0, L is such that effectively a few states with energies up to $aE \approx 1$ contribute, the x_0-dependence may again be strong and cutoff effects may be enhanced. However, the enhancement will not be as large as in Sect. 2.1 since there is no singular dependence at small x_0. In Sect. 3 we will see quantitatively how the behaviour changes as L and x_0 are increased starting from $L, x_0 \ll 1/\Lambda$.

We remark that the foregoing discussion is of course not in contradiction to the perturbative behaviour. In the perturbative region, x_0 is small and many states contribute significantly. But asymptotic freedom implies that their coefficients w_{nm} are fine-tuned such as to produce the smooth behaviour of eq. (2.8). This is often called quark-hadron duality.

2.3 Energies and matrix elements

The most common application of Symanzik's effective theory is to energies and matrix elements, e.g. extracted from eq. (2.9) at large x_0. The expansion of such observables,

$$O_{\mathrm{lat}} \sim O_{\mathrm{cont}} + a\, s_1 \,+\, a^2\, s_2 + \ldots\,, \tag{2.10}$$

will be valid and accurate when the relevant energies, momenta and masses are small compared to a^{-1}. For the O(a)-improved theory, a first scaling test [15] showed that indeed the corrections to the continuum appear to be reasonably small when $a \leq 0.1\,\mathrm{fm}$.

3 The Schrödinger functional correlator $f^{\rm P}_{\rm lat}$

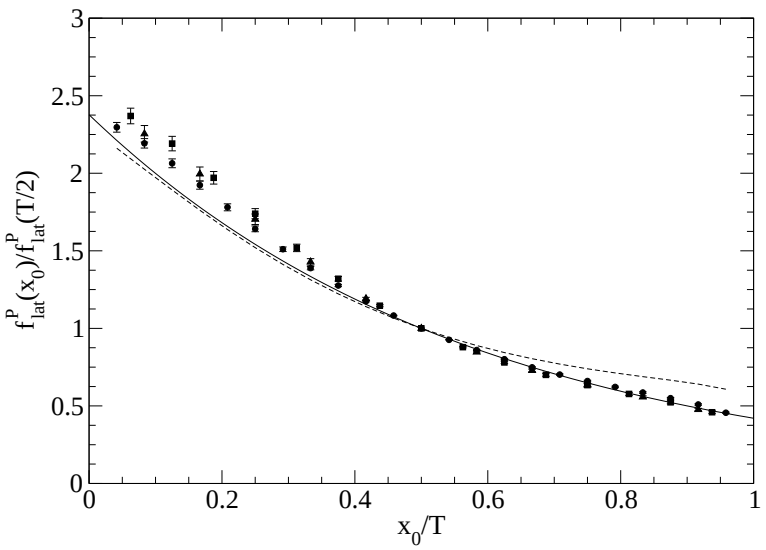

Figure 1: *The correlator $f^{\rm P}_{\rm lat}$ in the perturbative region, $L \leq 0.5\,$fm. The continuous curve shows the tree-level behaviour, while data points are for $\bar{g}^2(L/2) = 3.33$ (or $\bar{g}^2(L) \approx 5.5$) with filled circles for $L/a = 24$, squares for $L/a = 16$ and triangle for $L/a = 12$. A dashed line shows the position of the data with $\bar{g}^2(L/2) = 1.50$, $L/a = 24$.*

We now proceed to discuss numerical results for $f_{\rm P}$ in different regions of L (or $\bar{g}^2(L)$). Let us start from the short distance, weak coupling, region. In the non-perturbative computation of the scale-dependence of composite operators, such as P^a, our collaboration chose Schrödinger functional boundary conditions with $\theta = 0.5$, $T = L$ and a vanishing background field [12]. From these simulations we have precise data for $f^{\rm P}_{\rm lat}$ in a range of the Schrödinger functional coupling $0.98 \leq \bar{g}^2(L) \leq 5.5$ [11, 12]. In order to cancel the renormalization factor $Z_{\rm P}$, we normalize by $f^{\rm P}_{\rm lat}$ at the midpoint, $x_0 = T/2 = L/2$.

At $\bar{g}^2 = 0$, eq. (2.8) yields the slowly falling exponential plotted in Figure 1 as a continuous curve. The non-perturbative results at $\bar{g}^2(L) \approx 5.5$ are next to this tree-level curve, even though in general perturbation theory is not very accurate at this coupling. For example the renormalization factor $Z_{\rm P}$ is known to be a factor 2 away from one. We note in passing that the *very* close agreement with tree-level at $x_0/T \geq 1/2$ is somewhat accidental, as e.g. at a weak coupling of $\bar{g}^2(L/2) = 1.50$ the curve is some 15 % away (dashed line). All in all, the smooth behaviour anticipated in our general discussion, is found to a remarkable degree in the whole range of $L \lesssim 0.5\,$fm. Cutoff effects are very small. Even at the shortest distances, x_0/a, the a^2 effects are only a few percent at $\bar{g}^2(L) = 5.5$. At weaker coupling, $\bar{g}^2(L/2) = 1.50$, the a^2 effects are

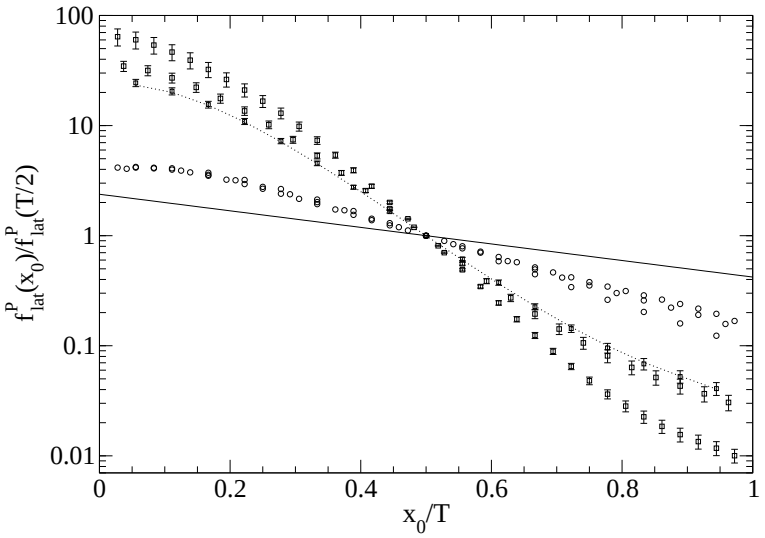

Figure 2: *The correlator $f^{\rm P}_{\rm lat}$ for $L \approx 0.8\,$fm, $T \approx 1.8\,$fm, $\theta = 0.5$ is represented by squares. $L/a = 8, 12, 16$ data increase at small x_0. A dotted line indicates the location of $\theta = 0, L/a = 8$. Circles show the behaviour at $L \approx 1.2\,$fm, $T \approx 1.8\,$fm, $\theta = 0$. Their errors are of the order of the symbol size.*

invisible within our precision of $\approx 2\%$ (the data are not plotted in order not to clutter the graph). As explained in the previous section, this behaviour of the Schrödinger functional correlators goes hand in hand with small cutoff effects in the step scaling functions which describe for example the running of coupling and quark mass [12].

In physical units we have thus far investigated the region $L = T \lesssim 0.5\,$fm. For L just somewhat larger, $L = 0.8\,$fm, $T = 9/4\,L$, and $\theta = 0$, we have previously observed significant a^2 effects in our computation of $Z_{\rm A}$ [10]. They were prominent in the statistically significant disconnected contributions to $Z_{\rm A}$, which can be shown to vanish in the continuum limit. As a consequence $Z_{\rm A}$ determined with or without the disconnected diagrams differed by almost 15% at $a \approx 0.1\,$fm. Although the disconnected diagrams vanish quickly as a is reduced, an unpleasantly large ambiguity remained at typical values of a. For details we refer to the quoted reference.

We now turn to that same kinematics and subsequently to larger L. But first we point out that in this region the dependence of $f^{\rm P}_{\rm lat}(x_0)/f^{\rm P}_{\rm lat}(T/2)$ on θ is insignificant compared to the effects we will discuss. An explicit example is provided by comparing the dotted line of Figure 2 with the $L/a = 8$ data points. For our numerical demonstration we will thus freely use data at available values of θ.

We start with correlation functions $f^{\rm P}_{\rm lat}$ at the same parameters as in [10], except for that we remain with $\theta = 0.5$. The behaviour of $f^{\rm P}_{\rm lat}$, plotted in Figure 2, differs drastically from Figure 1 – see the tree-level curve as a reference. The non-perturbative correlators drop steeply (note that we use a logarithmic scale) and follow the characteristics of the described intermediate regime, where neither the smooth perturbative behaviour is

realized, nor a single intermediate state is dominating (the latter would be seen as a straight line in the figure). For the coarsest lattice the logarithmic slope (effective mass) at $x_0 = T/2$ is as high as 0.8 in lattice units. In this situation, we find indeed very significant lattice spacing effects. It is then not surprising that there are also large a^2 effects in the form of the mentioned disconnected diagrams.

For an improved determination of $Z_{\rm A}$, we would like to choose a kinematical region, where (1) the a^2 effects are better suppressed and (2) the Schrödinger functional simulations can be done close to or in the chiral limit. The simulations can reach the chiral limit when the infrared cutoff on the spectrum of the Dirac operator is sufficiently large. Since in the Schrödinger functional the infrared cutoff is dominantly controlled by $1/T$, we do not want to increase T significantly compared to the previous $T \approx 1.8\,\mathrm{fm}$. On the other hand, the energies E_n^π are expected to be decreasing with L; in fact in the small L limit they scale as L^{-1}. This leads us to consider a somewhat larger L, namely $L \approx 1.2\,\mathrm{fm}$. Also in such a situation, namely with $T = 3/2\,L$, we have simulation results [26], generated for the determination of improvement coefficients $b_{\rm m}$, $b_{\rm A} - b_{\rm P}$ as well as the renormalization of the bare mass $m_{\rm q}$ following ref. [27]. The circles in Figure 2 show $f_{\rm lat}^{\rm P}$ in this kinematical situation[2]. The function has a much slower decay and indeed only moderate lattice artifacts. The energies of the states dominating the correlator appear to be significantly lower – at least the logarithmic slope never exceeds a value of 0.3 at the coarsest lattice spacing.

This kinematics is a good starting point for a redetermination of the renormalization factor $Z_{\rm A}$ with reduced intrinsic a^2 ambiguities.

4 New determination of $Z_{\rm A}$

The renormalization condition of the axial current is obtained by considering an axial Ward identity in exactly the same way as it was done in ref. [10]. One starts from a Schrödinger functional correlation function of the axial current with two pseudo-scalar boundary operators,

$$\mathcal{O}^a(\omega) = \frac{a^6}{L^3}\sum_{\mathbf{x},\mathbf{y}} \overline{\zeta}(\mathbf{x})\gamma_5 \tfrac{1}{2}\tau^a \omega(\mathbf{x}-\mathbf{y})\zeta(\mathbf{y}) \tag{4.1}$$

$$\mathcal{O}'^a(\omega) = \frac{a^6}{L^3}\sum_{\mathbf{x},\mathbf{y}} \overline{\zeta}'(\mathbf{x})\gamma_5 \tfrac{1}{2}\tau^a \omega(\mathbf{x}-\mathbf{y})\zeta'(\mathbf{y}) \tag{4.2}$$

and performs an axial rotation of the variables in a region around the axial current [28]. Using isospin symmetry and PCAC one obtains for vanishing quark mass the Ward identity

$$Z_{\rm A}^2 f_{\rm AA}^{\rm I}(x_0, y_0, \omega) = f_1(\omega) + \mathrm{O}(a^2)\,, \quad x_0 > y_0\,, \tag{4.3}$$

[2] At $L/a = 12$ the massless point is not reached, but the behaviour at the smallest mass, shown here, does not change significantly when the mass is increased. See Sect. 4 for details.

in terms of the correlation function

$$f_{\rm AA}^{\rm I}(x_0,y_0,\omega) = -\tfrac{a^6}{6}\sum_{\mathbf{x},\mathbf{y}}\epsilon^{abc}\epsilon^{cde}\Big\langle \mathcal{O}'^d(\omega)\,(A_{\rm I})_0^a(x)\,(A_{\rm I})_0^b(y)\,\mathcal{O}^e(\omega)\Big\rangle\,, \qquad (4.4)$$

$$f_1(\omega) = -\tfrac{1}{3}\langle \mathcal{O}'^a(\omega)\,\mathcal{O}^a(\omega)\rangle\,. \qquad (4.5)$$

The superscript I reminds us that the improved axial current

$$(A_{\rm I})_\mu^a = A_\mu^a + ac_{\rm A}\widetilde{\partial_\mu}P^a\,, \quad A_\mu^a(x) = \overline{\psi}(x)\gamma_\mu\gamma_5\tfrac{1}{2}\tau^a\psi(x)\,, \qquad (4.6)$$

is to be inserted. We refer to section 2 in ref. [10] for a derivation, the exact lattice implementation as well as a generalization to finite mass, which we use.

Compared to that work we only change the kinematics. First of all the computation is now performed on a lattice of size $L \simeq 1.2$ fm instead of 0.8 fm, as motivated in the previous sections. Secondly, together with the sources $\mathcal{O}^a$, eq. (2.5), and $\mathcal{O}'^a$, which correspond to $\omega_0(\mathbf{x}) = 1$, we consider the following basis of wave-functions

$$\omega_i(\mathbf{x}) = N_i^{-1}\sum_{\mathbf{n}\in\mathbf{Z}^3}\overline{\omega}_i(|\mathbf{x}-\mathbf{n}L|)\,,\ i=1,2,3\,, \qquad (4.7)$$

$$\overline{\omega}_1(r) = \mathrm{e}^{-r/a_0}\,, \quad \overline{\omega}_2(r) = r\,\mathrm{e}^{-r/a_0}\,, \quad \overline{\omega}_3(r) = \mathrm{e}^{-r/(2a_0)}\,,$$

in order to construct the external operators. Here, we keep the physical length scale a_0 fixed in units of L by choosing $a_0 = L/6$ and the (dimensionful) coefficients N_i are set to normalize the wave function via $a^3\sum_{\mathbf{x}}\omega_i^2(\mathbf{x}) = L^3$. The same set of interpolating fields, for the same L, has been used in ref. [29] to determine the improvement coefficient $c_{\rm A}$ by requiring the quark mass derived from the PCAC Ward identity to stay the same as the external states are changed. We therefore choose the already determined [29] optimal wave-function

$$\omega_{\pi^{(0)}} = \sum_{i=1}^{3}\eta_i^{(0)}\omega_i\,, \quad \eta^{(0)} = (0.5172,\ 0.6023,\ 0.6081)\,. \qquad (4.8)$$

It suppresses the contribution of the first excited state in the pseudoscalar channel to the correlation functions under consideration (see section 2 in ref. [29]).

The final result will turn out to differ significantly from the determination in ref. [10] at the two largest couplings only. We therefore did not recompute $Z_{\rm A}$ for small couplings and rather use the old estimates.

4.1 Results

We have two dynamical flavors of non-perturbatively improved Wilson quarks [30] and the plaquette gauge action. The improvement coefficients $c_{\rm sw}, c_{\rm A}$ were set to their non-perturbative values [29, 30]. We chose $T = 3/2L$ with periodic boundary conditions ($\theta = 0$) in space and vanishing background field. We used the HMC algorithm with two

pseudo-fermion fields as proposed in refs. [1, 31]. The particular implementation has been discussed and tested in refs. [32] and [33]. Following the last reference we chose a trajectory length of $\tau = 2$ except for at $\beta = 5.2$ where we set $\tau = 1$.

The normalization factor $Z_{\rm A}$ is given by [10]

$$Z_{\rm A}(g_0^2) = \lim_{m\to 0} \sqrt{f_1(\omega)} \left[f_{\rm AA}^{\rm I}(2T/3, T/3, \omega) - 2m\tilde{f}_{\rm PA}^{\rm I}(2T/3, T/3, \omega) \right]^{-1/2} . \qquad (4.9)$$

The definition of $\tilde{f}_{\rm PA}^{\rm I}(2T/3, T/3, \omega)$ and the PCAC quark mass m can be found in ref. [10]. After performing the Wick contractions one realizes that disconnected quark diagrams, where no propagator connects the two boundaries, contribute to $f_{\rm XY}^{\rm I}(x_0, y_0, \omega)$. These can be shown to vanish in the continuum massless limit as a consequence of the conservation of the axial current [10]. In an improved theory they therefore amount to $\mathrm{O}(a^2)$ effects on $Z_{\rm A}$. By dropping them one obtains an alternative definition of $Z_{\rm A}$, denoted $Z_{\rm A}^{\rm con}$. With the kinematics of ref. [10] the difference between $Z_{\rm A}$ and $Z_{\rm A}^{\rm con}$ for $\beta = 6/g_0^2 < 5.5$ was found to be rather large, though consistent with $\mathrm{O}(a^2)$ scaling. As it will become clear in the following this effect is very small in the computation presented here, which therefore significantly improves on the result in ref. [10].

In order to ensure a smooth dependence of $Z_{\rm A}$ on the bare coupling g_0^2 and the correct scaling of discretization errors proportional to a^2, we impose our normalization condition on a line of constant physics. This requires keeping all length scales fixed as g_0^2 is varied. The lattice size L is set to approximately $1.8L^*$ with L^* given by the condition $\bar{g}^2(L^*) = 5.5$, where $\bar{g}^2(L)$ is the Schrödinger functional coupling defined in refs. [11, 24]. The relation between $\frac{L^*}{a}$ and g_0 could be taken from ref. [34].

The bare parameters of our simulations and the results for $Z_{\rm A}$ are collected in Table 1. Due to algorithmic instabilities caused by the appearance of very small,

				$\omega = \omega_0$		$\omega = \omega_{\pi(0)}$	
L/a	β	κ	am	$Z_{\rm A}$	$Z_{\rm A}^{\rm con}$	$Z_{\rm A}$	$Z_{\rm A}^{\rm con}$
12	5.2	0.1355	0.02121(36)	0.788(15)	0.784(4)	0.784(16)	0.7874(35)
12	5.2	0.1357	0.01434(48)	0.775(10)	0.769(4)	0.777(11)	0.7703(36)
12	5.2	0.1358	0.00907(39)	0.776(8)	0.777(4)	0.776(9)	0.7788(37)
12	5.2		$\to 0$	0.766(18)	0.773(15)	0.769(20)	0.774(16)
16	5.4	0.136645	0.00062(26)			0.779(5)	0.793(5)
24	5.7	0.136704	0.00072(14)			0.808(5)	0.802(3)

Table 1: *Bare parameters and simulation results (statistical errors only). At $\beta = 5.2$ the value of the renormalization constant extrapolated to the chiral limit is reported in the fourth line including the associated systematic uncertainty (see text for details). The number of decorrelated measurements used varies between 1200 (at $\beta = 5.2$) and 200 (at $\beta = 5.7$).*

unphysical, eigenvalues in the spectrum of the Wilson-Dirac (SF) operator [3,35], at the coarsest lattice spacing we could simulate down to bare quark masses of about $a\,m \approx$

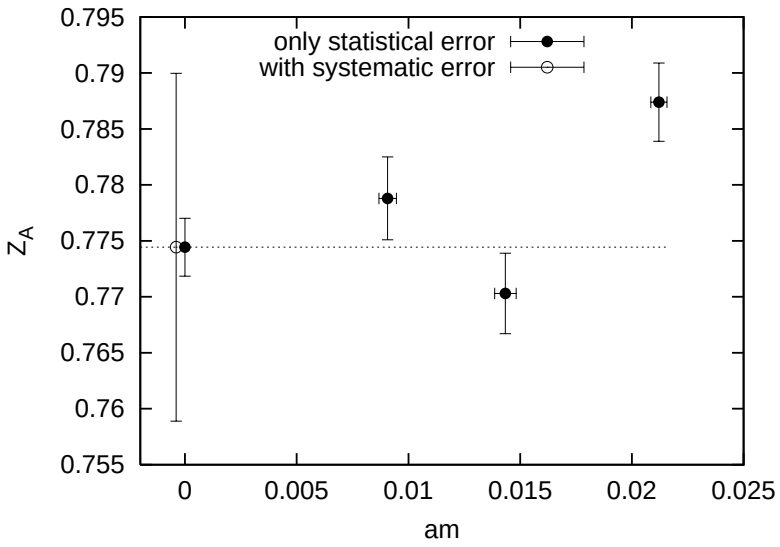

Figure 3: *Estimate of $Z_{\rm A}^{\rm con}$ at the chiral point for $\beta = 5.2$. The error-bar of the filled circle at $am = 0$ shows the statistical error whereas the error on the open circle includes our estimate of the* O(am) *systematic uncertainty.*

0.01 only. Our estimates for the massless limits at $\beta = 5.2$ are just weighted averages of the numbers at the two lightest quark masses. The errors in Table 1 include a systematic uncertainty for possible O(am) contaminations given by the difference between the determination at the heaviest mass and the described estimate. This uncertainty is added linearly to the statistical error. A similar O(am) uncertainty would be obtained by comparing to a linear fit in am with all three points. Figure 3 illustrates the procedure for $Z_{\rm A}^{\rm con}$ and $\omega = \omega_{\pi^{(0)}}$. It is clear from the plot that the dependence of $Z_{\rm A}$ on the quark mass is rather mild as expected for the "massive"definition of the renormalization constant [10] used here. Similar remarks obviously apply to the case $\omega = \omega_0$, as Table 1 shows that the two wave-functions give consistent results for all values of κ. At the other values of the bare coupling we simulated at very small quark masses. Given also the flat dependence observed at $\beta = 5.2$ we did not need to estimate an effect of order am. As anticipated, already at $\beta = 5.7$ the present result nicely agrees with the numbers in ref. [10]. Conversely, at $\beta = 5.2$ the new determination of $Z_{\rm A}$ is about 8% larger than the old one. These comparisons are summarized in Figure 4.

In view of the above discussion we smoothly interpolate the data for $Z_{\rm A}^{\rm con}$ and $\omega = \omega_{\pi^{(0)}}$in the region $5.2 \leq \beta \leq 5.7$ and those in ref. [10] for $7.2 \leq \beta \leq 9.6$ (filled circles in Figure 4) by the formula

$$Z_{\rm A}(g_0^2) = 1 - 0.116 g_0^2 + 0.011 g_0^4 - 0.072 g_0^6 \ , \tag{4.10}$$

where the coefficient of the term linear in g_0^2 is fixed by 1-loop perturbation theory [36] and the last two coefficients are the result of a fit. We ascribe an absolute error to $Z_{\rm A}$,

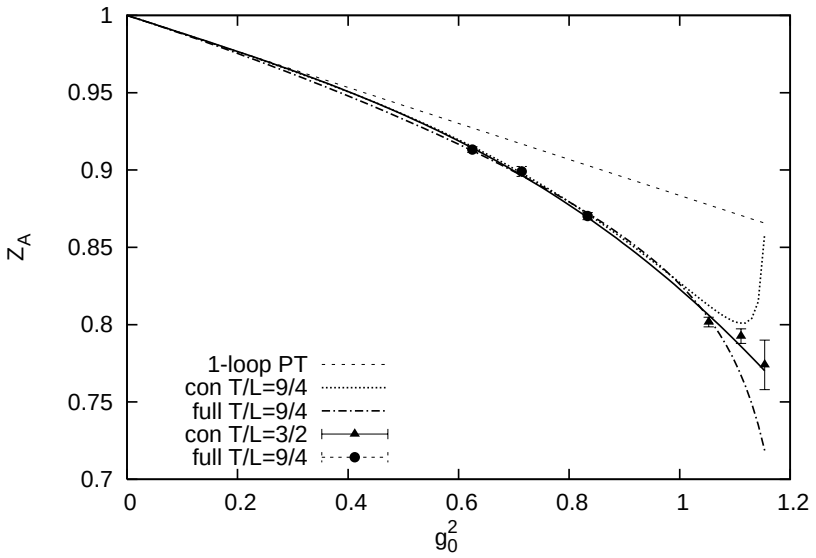

Figure 4: *Comparison of the new results for $Z_{\rm A}^{\rm con}$ with the old ones for $Z_{\rm A}$ and $Z_{\rm A}^{\rm con}$ in ref. [10]. The solid curve represents the interpolation formula in eq. (4.10).*

which decreases from 0.016 at $\beta = 5.2$ over 0.005 at $\beta = 5.4$ to 0.003 for $\beta \geq 5.7$. We note that our systematic O(am) error at $\beta = 5.2$ is rather conservative, see Fig. 3.

4.2 Other renormalization conditions of the axial current

In order to get a further impression about residual cutoff effects, we also studied an alternative definition of $Z_{\rm A}$. It is obtained in the same framework by replacing a light quark with a static one in the external operators $\mathcal{O}$ and $\mathcal{O}'$. By remaining with the flat wave-function and by denoting the static quark field on the boundary $x_0 = 0$ by $\zeta_{\rm h}$ we write

$$\mathcal{O}_i^{\rm hl} = \frac{a^6}{L^3} \sum_{\mathbf{x},\mathbf{y}} \overline{\zeta}_{\rm h}(\mathbf{x})\gamma_5\zeta_i(\mathbf{y})\,, \qquad \mathcal{O}_i'^{\rm hl} = \frac{a^6}{L^3} \sum_{\mathbf{x},\mathbf{y}} \overline{\zeta}_i'(\mathbf{x})\gamma_5\zeta_{\rm h}'(\mathbf{y})\,, \tag{4.11}$$

where $i = 1, 2$ is a flavour index. The flavour contractions in $f_{\rm XY}^{\rm I}$ are changed correspondingly. The correlator $f_{\rm AA}^{\rm hl,I}$ for example is written

$$f_{\rm AA}^{\rm hl,I}(x_0, y_0) \;=\; -\frac{ia^6}{6} \sum_{\mathbf{x},\mathbf{y}} \epsilon^{abc} \langle \mathcal{O}_i'^{\rm hl} (A_{\rm I})_0^a(x)\, (A_{\rm I})_0^b(y) \tfrac{1}{2}(\tau^c)_{ij} \mathcal{O}_j^{\rm hl} \rangle \tag{4.12}$$

and the massless normalization condition becomes

$$Z_{\rm A}^2\, f_{\rm AA}^{\rm hl,I}(2T/3, T/3) = f_1^{\rm hl} + {\rm O}(a^2)\,, \tag{4.13}$$

with

$$f_1^{\rm hl} = -\frac{1}{8}\,\langle \mathcal{O}_i'^{\rm hl}\mathcal{O}_i^{\rm hl}\rangle\ . \tag{4.14}$$

As the fields X and Y in the correlator do not contain static fields, it is clear that disconnected diagrams cannot appear and the static quark propagates from one boundary to the other. Static quarks are discretized through the HYP1 and HYP2 static-quark actions [37], which have a relatively good signal to noise ratio in static-light correlation functions at large time separations.

L/a	T/a	β	κ	am	θ	$Z_{\rm A}$ [HYP1]	$Z_{\rm A}$ [HYP2]
12	18	5.2	0.1355	0.02121(36)	0	0.7904(66)	0.7882(55)
12	18	5.2	0.1357	0.01434(48)	0	0.7729(79)	0.7734(73)
12	18	5.2	0.1358	0.00907(39)	0	0.7731(75)	0.7736(70)
8	18	5.2	0.1357	0.00662(75)	0.5	0.8284(80)	0.8285(66)
8	18	5.2	0.1358	0.00325(82)	0.5	0.8252(94)	0.8206(82)

Table 2: *Simulations parameters and results for the alternative "static" definition of* $Z_{\rm A}$.

The check was performed at the largest lattice spacing where ambiguities are expected to be most pronounced. Simulation parameters and results are collected in Table 2. The results at $L \simeq 1.2$ fm agree with those in the previous section, indicating again small overall cutoff effects. The values at $L \simeq 0.8$ fm instead again suggest that the determination in ref. [10] suffers from large a^2 effects, as both $Z_{\rm A}$ and $Z_{\rm A}^{\rm con}$ there differ significantly (and especially for small quark masses) from the numbers in Table 2.

4.3 Renormalization of the vector current

We also recomputed the renormalization constant $Z_{\rm V}$ of the vector current in the new kinematics. Since it changes by less than 2% compared to ref. [10] at the largest lattice spacing, there is no reason to publish a new determination.

5 Conclusions

We have discussed possible kinematical enhancements of cutoff effects in lattice gauge theory determinations of QCD correlation functions. In this respect, the typical SF correlation functions improve significantly over those of composite local fields with periodic boundary conditions (or large volume). The origin of this difference is simply the difference in mass dimensions of the Schrödinger functional boundary fields compared to the usual local composite fields. Since the latter is at least three, time-slice correlators diverge at least as x_0^{-3} at short distances. Such a steep behavior is difficult to approximate in a discretized theory.

In the Schrödinger functional we identified a parametrically much weaker, but still relevant, kinematical enhancement of cutoff effects. It appears in the transition region

between approximately perturbative behaviour and dominantly non-perturbative one. Numerically we find that it appears e.g. for a $T \times L^3$ geometry with $L \approx 0.8\,\mathrm{fm}$, $T \approx 1.8\,\mathrm{fm}$. In this kinematical situation a few hadronic intermediate states are relevant for the correlators and can produce a relatively steep decay of correlation functions even at a small quark mass.

This means that the transition region from approximately perturbative to strongly non-perturbative is a relatively difficult one for numerical simulations. Discretization errors have to be investigated carefully. Fortunately we also saw that this region is rather narrow. With the step scaling method [19, 20, 22] it is typically bridged by one step.

Avoiding the difficult region in the renormalization condition for the relativistic axial current, we have finally presented a significant improvement of the previous determination of Z_A [10]. The difference to the old one is of order a^2, but it is up to 10 % at the largest lattice spacing considered. In our new determination we find that disconnected contributions, which can be shown to vanish in the continuum limit, are very small – in contrast to the previous kinematical setup [10]. We also see a nice agreement with a renormalization condition where a static quark is present as a spectator in the Ward identity. The previous determination of Z_V is confirmed.

Acknowledgements. We thank Roland Hoffmann for his collaboration in this project in an early phase and Ulli Wolff for comments on a first draft of the paper. We acknowledge useful discussions with Martin Lüscher and Ulli Wolff and thank our colleagues G. de Divitiis, P. Fritzsch, J. Heitger, N. Tantalo and R. Petronzio for collaborating on the generation of some of the Schrödinger functional gauge configurations. We thank NIC for allocating computer time on the APE computers at DESY Zeuthen to this project and the APE group for its help. This work is supported by the Deutsche Forschungsgemeinschaft in the SFB/TR 09 and by the European community through EU Contract No. MRTN-CT-2006-035482, "FLAVIAnet".

References

[1] M. Hasenbusch, *Speeding up the Hybrid-Monte-Carlo algorithm for dynamical fermions*, *Phys. Lett.* **B519** (2001) 177–182, [hep-lat/0107019].

[2] M. Lüscher, *Schwarz-preconditioned HMC algorithm for two-flavour lattice QCD*, *Comput. Phys. Commun.* **165** (2005) 199, [hep-lat/0409106].

[3] L. Del Debbio, L. Giusti, M. Lüscher, R. Petronzio, and N. Tantalo, *Stability of lattice QCD simulations and the thermodynamic limit*, *JHEP* **02** (2006) 011, [hep-lat/0512021].

[4] M. Lüscher, *Deflation acceleration of lattice QCD simulations*, *JHEP* **12** (2007) 011, [0710.5417].

[5] L. Del Debbio, L. Giusti, M. Lüscher, R. Petronzio, and N. Tantalo, *QCD with light Wilson quarks on fine lattices. II: DD-HMC simulations and data analysis*, *JHEP* **02** (2007) 082, [hep-lat/0701009].

[6] **ETM** Collaboration, P. Boucaud *et al.*, *Dynamical twisted mass fermions with light quarks*, *Phys. Lett.* **B650** (2007) 304–311, [hep-lat/0701012].

[7] Y. Kuramashi, $N_f = 2 + 1$ *dynamical Wilson quark simulation toward the physical point*, *PoS* **LAT2007** (2007) 017, [0711.3938].

[8] S. Dürr *et al.*, *Scaling study of dynamical smeared-link clover fermions*, 0802.2706.

[9] **ALPHA, JLQCD and CPPACS** Collaboration, R. Sommer *et al.*, *Large cutoff effects of dynamical Wilson fermions*, *Nucl. Phys. Proc. Suppl.* **129** (2004) 405–407, [hep-lat/0309171].

[10] M. Della Morte, R. Hoffmann, F. Knechtli, R. Sommer, and U. Wolff, *Non-perturbative renormalization of the axial current with dynamical Wilson fermions*, *JHEP* **07** (2005) 007, [hep-lat/0505026].

[11] **ALPHA** Collaboration, M. Della Morte *et al.*, *Computation of the strong coupling in QCD with two dynamical flavours*, *Nucl. Phys.* **B713** (2005) 378–406, [hep-lat/0411025].

[12] **ALPHA** Collaboration, M. Della Morte *et al.*, *Non-perturbative quark mass renormalization in two-flavor QCD*, *Nucl. Phys.* **B729** (2005) 117–134, [hep-lat/0507035].

[13] M. Della Morte, P. Fritzsch, and J. Heitger, *Non-perturbative renormalization of the static axial current in two-flavour QCD*, *JHEP* **02** (2007) 079, [hep-lat/0611036].

[14] R. Sommer, *Non-perturbative QCD: Renormalization, $O(a)$-improvement and matching to heavy quark effective theory*, hep-lat/0611020.

[15] **ALPHA** Collaboration, M. Della Morte *et al.*, *Scaling test of two-flavor $O(a)$-improved lattice QCD*, 0804.3383.

[16] K. Symanzik, *Continuum limit and improved action in lattice theories. 1. Principles and ϕ^4 theory*, *Nucl. Phys.* **B226** (1983) 187.

[17] K. Symanzik, *Continuum limit and improved action in lattice theories. 2. O(N) nonlinear sigma model in perturbation theory*, *Nucl. Phys.* **B226** (1983) 205.

[18] M. Lüscher, S. Sint, R. Sommer, and P. Weisz, *Chiral symmetry and O(a) improvement in lattice QCD*, *Nucl. Phys.* **B478** (1996) 365–400, [hep-lat/9605038].

[19] M. Lüscher, P. Weisz, and U. Wolff, *A numerical method to compute the running coupling in asymptotically free theories*, *Nucl. Phys.* **B359** (1991) 221–243.

[20] M. Lüscher, R. Sommer, U. Wolff, and P. Weisz, *Computation of the running coupling in the SU(2) Yang-Mills theory*, *Nucl. Phys.* **B389** (1993) 247–264, [hep-lat/9207010].

[21] S. Sint, *On the Schrödinger functional in QCD*, *Nucl. Phys.* **B421** (1994) 135–158, [hep-lat/9312079].

[22] **ALPHA** Collaboration, S. Capitani, M. Lüscher, R. Sommer, and H. Wittig, *Non-perturbative quark mass renormalization in quenched lattice QCD*, *Nucl. Phys.* **B544** (1999) 669, [hep-lat/9810063].

[23] M. Lüscher, R. Narayanan, P. Weisz, and U. Wolff, *The Schrödinger functional: A renormalizable probe for nonabelian gauge theories*, *Nucl. Phys.* **B384** (1992) 168–228, [hep-lat/9207009].

[24] M. Lüscher, R. Sommer, P. Weisz, and U. Wolff, *A precise determination of the running coupling in the SU(3) Yang-Mills theory*, *Nucl. Phys.* **B413** (1994) 481–502, [hep-lat/9309005].

[25] **ALPHA** Collaboration, M. Guagnelli, J. Heitger, R. Sommer, and H. Wittig, *Hadron masses and matrix elements from the QCD Schrödinger functional*, *Nucl. Phys.* **B560** (1999) 465, [hep-lat/9903040].

[26] G. M. de Divitiis, P. Fritzsch, J. Heitger and N. Tantalo, in preparation.

[27] **ALPHA** Collaboration, M. Guagnelli *et al.*, *Non-perturbative results for the coefficients b_m and $b_A - b_P$ in O(a) improved lattice QCD*, *Nucl. Phys.* **B595** (2001) 44–62, [hep-lat/0009021].

[28] M. Lüscher, S. Sint, R. Sommer, and H. Wittig, *Nonperturbative determination of the axial current normalization constant in O(a) improved lattice QCD*, *Nucl. Phys.* **B491** (1997) 344–364, [hep-lat/9611015].

[29] M. Della Morte, R. Hoffmann, and R. Sommer, *Non-perturbative improvement of the axial current for dynamical Wilson fermions*, *JHEP* **03** (2005) 029, [hep-lat/0503003].

[30] **ALPHA** Collaboration, K. Jansen and R. Sommer, *O(a) improvement of lattice QCD with two flavors of Wilson quarks*, *Nucl. Phys.* **B530** (1998) 185–203, [hep-lat/9803017].

[31] M. Hasenbusch and K. Jansen, *Speeding up lattice QCD simulations with clover-improved Wilson fermions*, *Nucl. Phys.* **B659** (2003) 299–320, [hep-lat/0211042].

[32] **ALPHA** Collaboration, M. Della Morte *et al.*, *Simulating the Schrödinger functional with two pseudo- fermions*, *Comput. Phys. Commun.* **156** (2003) 62–72, [hep-lat/0307008].

[33] **ALPHA** Collaboration, H. B. Meyer *et al.*, *Exploring the HMC trajectory-length dependence of autocorrelation times in lattice QCD*, *Comput. Phys. Commun.* **176** (2007) 91–97, [hep-lat/0606004].

[34] M. Della Morte *et al.*, *Preparing for N_f=2 simulations at small lattice spacings*, *PoS* **LAT2007** (2007) 255, [0710.1263].

[35] **ALPHA** Collaboration, M. Della Morte, R. Hoffmann, F. Knechtli, and U. Wolff, *Impact of large cutoff-effects on algorithms for improved Wilson fermions*, *Comput. Phys. Commun.* **165** (2005) 49–58, [hep-lat/0405017].

[36] E. Gabrielli, G. Martinelli, C. Pittori, G. Heatlie, and C. T. Sachrajda, *Renormalization of lattice two fermion operators with improved nearest neighbor action*, *Nucl. Phys.* **B362** (1991) 475–486.

[37] M. Della Morte, A. Shindler, and R. Sommer, *On lattice actions for static quarks*, *JHEP* **08** (2005) 051, [hep-lat/0506008].